

Available online at [www.sciencedirect.com](http://www.sciencedirect.com)

SCIENCE @ DIRECT®

Vibrational Spectroscopy xxx (2005) xxx–xxx

VIBRATIONAL  
SPECTROSCOPY[www.elsevier.com/locate/vibspec](http://www.elsevier.com/locate/vibspec)

# Vibrational spectroscopic investigation of stereoregularity effects on syndiotactic polypropylene structure and morphology

Michael S. Sevegney<sup>a</sup>, Rangaramanujam M. Kannan<sup>a,\*</sup>, Allen R. Siedle<sup>b</sup>,  
Ratna Naik<sup>c</sup>, Vaman M. Naik<sup>d</sup>

<sup>a</sup> Department of Chemical Engineering and Materials Science, Wayne State University, Detroit, MI 48202-3902, USA

<sup>b</sup> 3M Company, St. Paul, MN 55144-1000, USA

<sup>c</sup> Department of Physics and Astronomy, Wayne State University, Detroit, MI 48201-3718, USA

<sup>d</sup> Department of Natural Sciences, Physics, University of Michigan-Dearborn, Dearborn, MI 48301-1491, USA

Received 28 October 2004; received in revised form 7 October 2005; accepted 17 October 2005

## Abstract

Vibrational spectroscopy is used to sensitively detect specific morphologies and microstructures present in metallocene-catalyzed syndiotactic polypropylenes (sPP). Six materials, ranging in racemic triad content from 26 to 96% *rr*, are studied. Changes in high-resolution infrared (IR) and Raman spectra of melt-slow-cooled films are observed as the degree of syndiotacticity varies. Three different types of peak behavior are observed: splitting, wavenumber shift, and change in peak intensity. An overall trend toward greater molecular order (e.g. ordered chain conformations, increased crystallinity) is observed as syndiotacticity increases. By combining results with supporting evidence from X-ray diffraction and IR linear dichroism experiments of highly syndiotactic sPP, new peak assignments are proposed for tacticity-sensitive vibrational bands. Some very interesting spectral behavior is observed for material of intermediate stereoregularity (49% *rr*). Previously unobserved peaks appear in X-ray diffractograms and IR absorbance spectra, suggesting the presence of an as-yet unidentified “transitional” structure—perhaps a disordered modification of crystalline Form I. This moderate level of syndiotacticity appears to be a critical point or threshold below which sPP chains are unable to adopt characteristic helical or planar zigzag conformations. Results from this work provide a more thorough understanding of stereochemical effects on vibrational spectra, which will be very useful in the interpretation of ongoing IR linear dichroism studies of newly available semi-syndiotactic (semi-sPP) materials.

© 2005 Elsevier B.V. All rights reserved.

**Keywords:** Syndiotactic poly(propylene) (sPP); FT-IR; Raman; Structure–property relationships; Metallocene catalysts

## 1. Introduction

As a tool for polymer analysis and characterization, vibrational spectroscopy has demonstrated utility beyond simple chemical “fingerprinting”. One such use is the collection of infrared (IR) absorbance difference spectra using multiply modulated, plane-polarized light in order to measure orientation anisotropy of individual components (e.g. chemical functionalities, microstructures, crystalline and amorphous domains) within complex polymeric materials. Specifically, the viscoelastic orientation and relaxation anisotropy of many

different materials have been characterized using infrared linear dichroism (IRLD) spectroscopy [1–12] and polarized Raman scattering [13,14]. IR and Raman spectra are sensitive to the local environment of polymer chains. Specifically, the shape, location, and intensity of a given peak can be affected if the corresponding vibrational moment experiences changes in its immediate surroundings due to:

1. The degree of order, on several scales:
  - a. Intramolecular—configuration of adjacent repeat units; affects the ability of a chain to adopt a conformation.
  - b. Intermolecular—secondary forces between conformed chains; affects the ability of material to crystallize.
  - c. Macromolecular crystallinity, paracrystalline aggregation, microscale and nanoscale domains.

\* Corresponding author. Tel.: +1 313 577 3879; fax: +1 313 577 3810.

E-mail address: [rkannan@che.eng.wayne.edu](mailto:rkannan@che.eng.wayne.edu) (R.M. Kannan).

2. Physical perturbation, especially thermal (near transition temperatures) and mechanical.

In order to analyze and interpret spectra properly, effects of each aforementioned variable must be distinguished from the others. This provides part of the impetus for the present work. Additional motivation for this undertaking comes from the recent availability of a new class of materials that has yet to be characterized thoroughly using vibrational spectroscopy.

Syndiotactic polypropylene (sPP) is a semicrystalline, thermoplastic elastomer with physical properties intermediate to the fully isotactic and atactic isomers. While a rich polymorphism was predicted for sPP many decades ago [15–17], the ability to synthesize, and thus to study experimentally, highly stereoregular sPP was only realized around 1990 with the advent of metallocene catalysts [18,19]. Since then, much has been learned regarding the crystal morphology [20–33], chain conformations [16,34–41], blend compatibility [42–44], elastomeric behavior [45–47], and many other physical properties of sPP. Vibrational spectroscopy has certainly contributed to experimental progress. IR absorbance [48–51] and Raman scattering [52,53] have been used to identify the presence and relative populations of (*gauche–gauche–trans–trans*), (*ggt*)<sub>n</sub>, helical and all-*trans*, (*tttt*)<sub>n</sub>, planar zigzag conformed chains as sPP undergoes a variety of thermal and mechanical processing conditions. Recently, infrared linear dichroism (IRLD) was used to probe component orientation and relaxation in tensile-deformed sPP [54,55]. Simultaneously collected absorbance and IRLD spectra reveal and quantify both the helical-to-planar-zigzag conformation change and “mesophase” [56] formation that accompany tensile yielding. The specific technique, rheo-optical FTIR spectroscopy [57] also provides a sensitive measure of stepwise changes in sPP while en route to completing a crystal-crystal transformation at greater strains (~600%) [58,59]. For the most part, studies have included sPP materials that possess a narrow range of stereoregularity. A rheo-FTIR investigation of “semi-syndiotactic” polypropylenes (semi-sPP’s) has been completed recently [60].

When controlled carefully, metallocene-catalyzed polymerization of propylene can yield materials with very well defined tacticity and molecular weight distributions. This has resulted in the development of semi-sPP [61,62] and “semi-isotactic” (isotactic–atactic stereoblock material, also known as elastomeric polypropylene or “ePP”) species [63,64], as well as high-molecular-weight (~10<sup>6</sup> g/mol) atactic polypropylene. Both semi-sPP and ePP possess excellent elastomeric properties at room temperature. A generally accepted physical description of elastomeric origins in both of these semicrystalline materials involves stereoregular crystallites, which provide mechanical strength, functioning as anchoring points for more stereoirregular amorphous chains that concurrently provide restorative forces, much like traditional cross-linked thermoset elastomers. Furthermore, the crystalline–amorphous interface has been characterized as a metastable mesophase, or mesomorphic domain, consisting of highly oriented, partially ordered (but not crystalline) chains that aggregate reversibly in

response to mechanical deformation [56]. The mesophase is thought to kinematically couple crystalline and amorphous domains during bulk deformation, thus imparting elastic behavior up to very high tensile strains. At this time, efforts to characterize ePP using rheo-FTIR spectroscopy are ongoing [65].

Some preliminary results on the mechanical and thermal behavior of semi-sPP have been published. Siedle uses single-pulse <sup>13</sup>C-NMR spectroscopy, modulated differential scanning calorimetry, and Raman spectroscopy to speculate on both the existence and importance of a peculiar crystalline–amorphous interfacial region (the aforementioned mesophase) with regard to enhanced mechanical behavior (versus a comparable atactic isomer) and reversible non-melting transitions at 50 and 70 °C [61]. De Rosa et al. have shown that poorly syndiotactic sPP possesses good elastic behavior at room temperature; however, the strain-induced crystal–crystal transformation and helical-to-planar-zigzag conformation change, both observed in highly syndiotactic sPP, are incomplete, even at very high strains (~700%) [66]. Hsu et al. have explored the effects of conformational [67] and configurational [68] defects on the Raman spectra of sPP. These works identify peaks that serve as good quantitative measurements of overall syndiotacticity and the relative populations of helical, planar zigzag, and amorphous chains. However, the poorest syndiotactic material used was only 52% *r* (racemic dyad content). The present work is an endeavor to address the effects of tacticity on the IR and Raman spectra of sPP. The goals of this work are two-fold:

1. Primarily, to begin resolving the effects of tacticity on IR and Raman spectra.
2. To possibly identify characteristic peaks of specific morphologies within sPP.

Valence force calculations, used to predict the vibrational spectra of sPP, have generated multiple groups of bands that are very close to one another in energy [69]. Therefore, it will be necessary to use high-resolution spectroscopy. In total, results for six different materials (ranging from approximately atactic to highly syndiotactic) are reported. Preparation, handling, and experimental parameters for all samples are carefully reproduced in an effort to ensure that tacticity is the lone variable.

## 2. Experimental

### 2.1. Materials

Five semi-syndiotactic polypropylenes (aPP, s-sPP32, s-sPP49, s-sPP65, s-sPP67), synthesized [70] using an *ansa*-metallocene catalyst [62], are analyzed. Highly stereoregular material (sPP) was obtained from the Fina Oil and Chemical Company. <sup>13</sup>C-NMR and high-temperature GPC-triple-detection were used to measure stereoregularity and molecular weight distributions, respectively, for each material. These

Table 1  
Stereoregularity and molecular weight distributions of semi-syndiotactic polypropylene materials

Material	% <i>rr</i>	% <i>rrrr</i>	% <i>mr</i>	% <i>mm</i>	$M_w$ (g/mol)	$M_n$ (g/mol)	PDI <sup>a</sup>
aPP	26.5	7.1	49.0	24.5	$1.16 \times 10^6$	$4.17 \times 10^5$	2.78
s-sPP32	32.0	11.1	41.4	26.6	$2.3 \times 10^5$	$6.1 \times 10^4$	3.8
s-sPP49	49.0	30.3	37.8	13.2	$3.5 \times 10^5$	$1.4 \times 10^5$	2.5
s-sPP65	65.4	49.4	24.3	10.3	$7.9 \times 10^5$	$2.2 \times 10^5$	3.6
s-sPP67	67.0	49.9	24.0	9.0	$2.3 \times 10^5$	$8.9 \times 10^4$	2.6
sPP	96				$2.285 \times 10^5$	$6.06 \times 10^4$	3.77

<sup>a</sup> Polydispersity index  $\equiv M_w/M_n$ .

results are reported in Table 1. All materials, except the approximately atactic species (aPP), have roughly similar molecular weight distributions.

Samples are prepared into film geometry of sufficient thickness for obtaining good results in all experimental methods. Bulk material is heated to 180 °C inside a hot press (Hydraulic Unit model 3912, Carver Inc.) and held for 20 min to ensure complete melting. Melts are then sandwiched between polytetrafluoroethylene sheets and compression molded into films of nearly uniform 150  $\mu\text{m}$  thickness. The pressing load is then removed and films are maintained 180 °C for 30 min to allow relaxation of any processing stresses [71]. Samples are then allowed to cool slowly to ambient temperature ( $\sim 30$  °C) over a period of 4 h. This step encourages the formation of any thermodynamically favorable ordered structures (e.g. conformed chains, aggregates, crystallites). It is expected that any structural order in each material will be composed mostly of chains adopting a  $(ggtt)_n$  helical bond sequence, a portion of which may contribute to crystalline Form I [22,24] in the more stereoregular species. Each sample film is allowed at least one month of residence at ambient conditions prior to testing. Under these processing conditions, it is unlikely that many macromolecular chains will adopt the less stable  $(ttt)_n$  planar zigzag conformation. However, it is unreasonable to expect that this conformation will be absent entirely, especially in more stereoregular samples.

## 2.2. Methods

High-resolution IR and Raman spectroscopy are used to characterize the overall composition of ordered structures within each melt-slow-cooled film. X-ray powder diffractometry is also used as a quick diagnosis of crystalline content. All experiments are performed at ambient temperature.

### 2.2.1. Fourier transform infrared (FTIR) spectroscopy

High-resolution absorbance spectra are collected using a Bio-Rad model FTS 6000 FTIR spectrometer operating in continuous scan mode. A silicon carbide source provides broadband excitation at mid-IR wavenumbers (4000–400  $\text{cm}^{-1}$ ). The Michelson interferometer uses a potassium bromide beamsplitter that rejects wavenumbers below 450  $\text{cm}^{-1}$ . Sample films are mounted with adhesive tape to an aluminum block suitable for transmission mode FTIR. Each scan is composed of 1024 co-added (averaged) transients collected at a resolution of 0.5  $\text{cm}^{-1}$ . While polypropylene IR peaks are inherently much broader, this level of resolution is

useful in quantifying small wavenumber shifts in peak centers that occur as syndiotacticity varies. Using these parameters and a deuterated triglycine sulfate (DTGS) detector necessitates a scan collection time of approximately 2 h.

### 2.2.2. Raman spectroscopy

Inelastic Stokes scattering spectra are collected using an unpolarized source at  $\sim 180^\circ$  (nearly backscattering geometry) with an *f*/6.4 TRIAX-550 Raman spectrometer (Jobin-Yvon Ltd.). The diffraction grating used has a groove density of 1200/mm, providing a spectral resolution slightly better than 4  $\text{cm}^{-1}$ . The entrance slit is set to a constant width of 0.2 mm. A krypton-argon ion laser (model 165/265, Spectra Physics Inc.) provides 400 mW of excitation at a wavelength of 514.5 nm. A liquid-nitrogen-cooled CCD detector system (Spectrum One Instruments, S.A.) is used to collect dispersed photons. Radiation counts are accumulated over an integration time of 15 s with five scans co-added. The spectrometer is calibrated using solid silicon and mercury vapor standards. If necessary, subsequently acquired sample spectra undergo a horizontal shift (wavenumber correction) equal to the difference between actual and tabulated Raman shift values for the calibration standards. SpectraMax software (Jobin-Yvon, Ltd. and Galactic Industries Corp.) is used both to compile and to process data from the detector and to control instrument parameters.

### 2.2.3. X-ray diffractometry

X-ray diffractograms are collected using a Rigaku RU2000 rotating anode powder diffractometer. It is equipped with a water-cooled copper target drum, a secondary beam graphite monochromator, and a scintillation counter detector. An acceleration tube voltage of 40 kV and current of 150 mA are used to generate characteristic Cu  $K\alpha_1$  photons (wavelength: 1.54056 Å). Sample films are affixed to an aluminum mount using adhesive tape. Datascan software is used to generate intensity versus Bragg angle plots from  $2\theta = 10\text{--}30^\circ$  at a sweep rate of 0.6°/min and a step size of 0.03°. Quantitative analysis is performed using the Jade software package.

## 3. Results and discussion

### 3.1. X-ray diffractometry

Diffractograms for all materials, ranging from a nearly atactic aPP to highly syndiotactic sPP, are shown in Fig. 1. The aPP and s-sPP32 traces are very similar, consisting of a broad

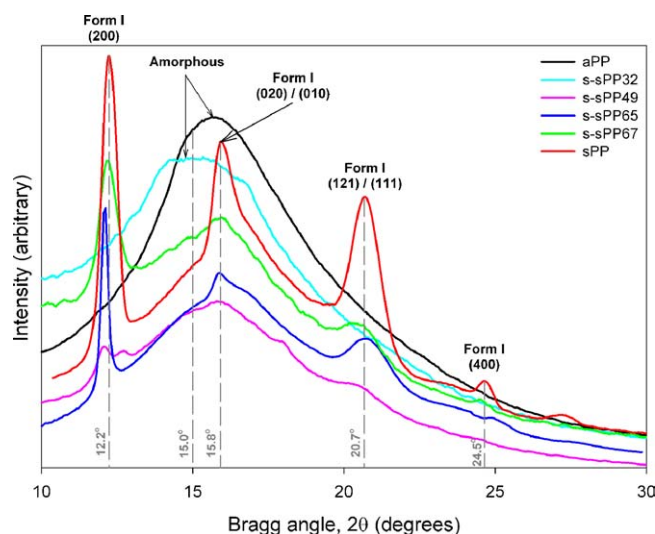


Fig. 1. Powder X-ray diffractograms of melt-slow-cooled semi-syndiotactic polypropylene films.

peak centered about  $2\theta = 15^\circ$ . The similitude to an amorphous background (i.e. broad, featureless traces) is expected for these materials, as their low degree of syndiotacticity is not conducive to crystallization. s-sPP65, s-sPP67, and sPP all show peaks characteristic of the disordered helical Form I crystal morph (orthorhombic, space group  $Pca_2$ ,  $a = 14.50 \text{ \AA}$ ,  $b = 5.60 \text{ \AA}$ ,  $c = 7.45 \text{ \AA}$ ) to some extent, with sPP including second-order peaks (see Table 2). The exact position of Form I peaks does vary slightly as syndiotacticity changes. Fig. 1 shows a general trend of peaks shifting to slightly greater Bragg

Table 2  
Crystallographic parameters for sPP polymorphs

Polymorph	$hkl$	$2\theta_{hkl} (^\circ)$	$d (\text{\AA})$
Helical (Forms I and II) <sup>c</sup>	2 0 0	12.193	7.25
	0 2 0 <sup>b</sup> /0 1 0 <sup>c</sup>	15.806	5.60
	2 1 1 <sup>d</sup>	18.805	4.71
	1 2 1 <sup>b</sup> /1 1 1 <sup>c</sup>	20.742	4.28
	0 0 2 <sup>a</sup>	23.859	3.73
	4 0 0 <sup>a</sup>	24.528	3.63
Form III <sup>f</sup>	0 2 0	15.849	5.59
	1 1 0	18.741	4.73
	0 2 1	23.699	3.75
	1 1 1	25.755	3.46
	1 2 1	29.290	3.05
	1 3 0	29.431	3.03
Mesophase <sup>g</sup>	1 1 0	16.990	5.21
	0 2 0	16.998	5.21
	1 0 1	22.959	3.87
	1 1 1	24.514	3.63

Bragg angles ( $2\theta_{hkl}$ ) given are for Cu  $K\alpha_1$  photons of wavelength  $1.54056 \text{ \AA}$ . Miller ( $hkl$ ) indices and interplanar spacing ( $d$ ) are given for each peak.

<sup>a</sup> Reflection is common to both Form I and Form II.

<sup>b</sup> Reflection is indexed based on limit-ordered Form I ( $b = 11.2 \text{ \AA}$ ).

<sup>c</sup> Reflection is indexed based on disordered Form I ( $b = 5.6 \text{ \AA}$ ).

<sup>d</sup> Reflection is unique to limit-ordered Form I ( $b = 11.2 \text{ \AA}$ ).

<sup>e</sup> Orthorhombic (space group  $C222_1$ ):  $a = 14.50 \text{ \AA}$ ,  $b = 5.60 \text{ \AA}$ ,  $c = 7.45 \text{ \AA}$ .

<sup>f</sup> Orthorhombic:  $a = 5.22 \text{ \AA}$ ,  $b = 11.17 \text{ \AA}$ ,  $c = 5.06 \text{ \AA}$ .

<sup>g</sup> Orthohexagonal:  $a = 6.02 \text{ \AA}$ ,  $b = 10.42 \text{ \AA}$ ,  $c = 5.05 \text{ \AA}$ .

angles as tacticity increases. For example, the peak representing the (2 0 0) planes of Form I shifts from  $12.0^\circ$  for s-sPP49 to  $12.2^\circ$  for sPP. This indicates shorter interplanar spacing, and thus, closer packing of chains along both  $a$ - and  $b$ -axes. This is intuitive, as a greater degree of molecular order is expected to enhance the strength of intermolecular interactions, thus allowing for, on average, a shorter equilibrium distance between crystalline chains. The s-sPP49 trace shows some evidence of Form I crystallization (at  $2\theta = 12^\circ$ ,  $20.7^\circ$ ). However, additional peaks appear at  $2\theta = 12.7^\circ$ ,  $17.9^\circ$  (shoulder), and  $23.0^\circ$  (shoulder) that are unique to this material. Limit disordered modifications of Form I (each possessing different crystallographic symmetry, and thus, different X-ray diffraction behavior) have been considered by De Rosa et al. [21,72–74] and Lovinger et al. [75]. However, the diffractogram of s-sPP49 does not fit well into any of the modifications proposed. It is suggested that this intermediate-tacticity material may be described as possessing some “transition” morphology that can increase in structural order as syndiotacticity increases. However, until a more thorough analysis can be performed on this material, it can only be speculated that s-sPP49, while capable of Form I crystallization, possesses enough stereoregularity to effect a highly non-ideal crystalline morphology.

### 3.2. Raman spectroscopy

Figs. 2–6 show Raman spectra of the polymers [76], in the Raman shift region from 200 to  $1500 \text{ cm}^{-1}$ . Since many vibrational modes inhabit each spectrum, the analysis to follow is divided into smaller wavenumber ranges, which are then discussed separately. Information on all vibrational peaks discussed is summarized in Table 3.

#### 3.2.1. 200–500 $\text{cm}^{-1}$ (Fig. 2)

The peak of greatest interest in this range is a “syndiotacticity index” band both calculated and observed experimentally by Hsu et al. [68]. The position of this peak varies between

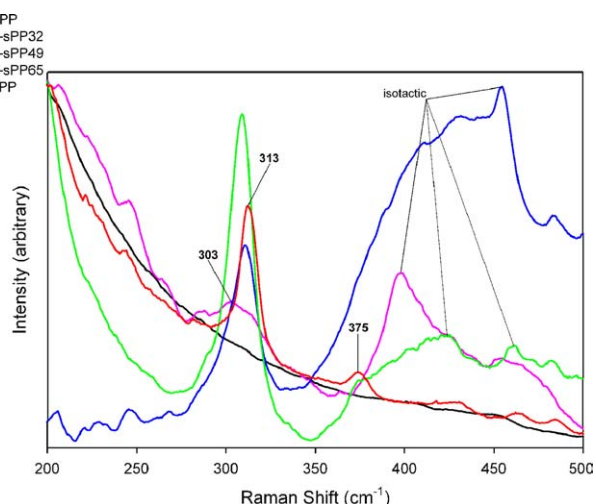


Fig. 2. Raman scattering spectra of melt-slow-cooled semi-syndiotactic polypropylene films in the Raman shift region from 200 to  $500 \text{ cm}^{-1}$ .

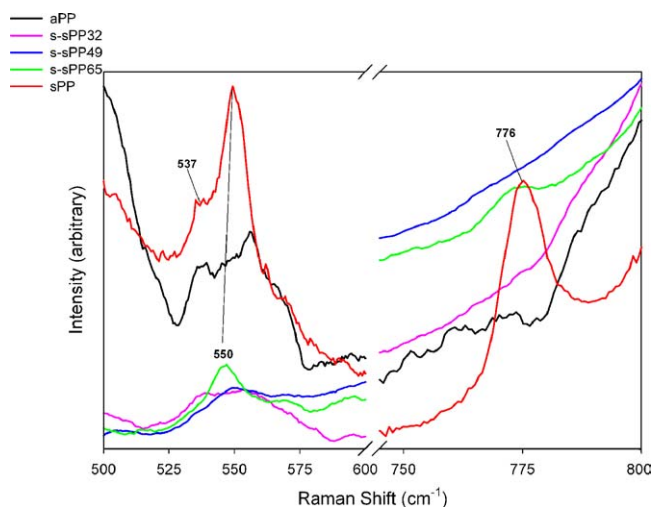


Fig. 3. Raman scattering spectra of melt-slow-cooled semi-syndiotactic polypropylene films in the Raman shift region from 500 to 800  $\text{cm}^{-1}$ .

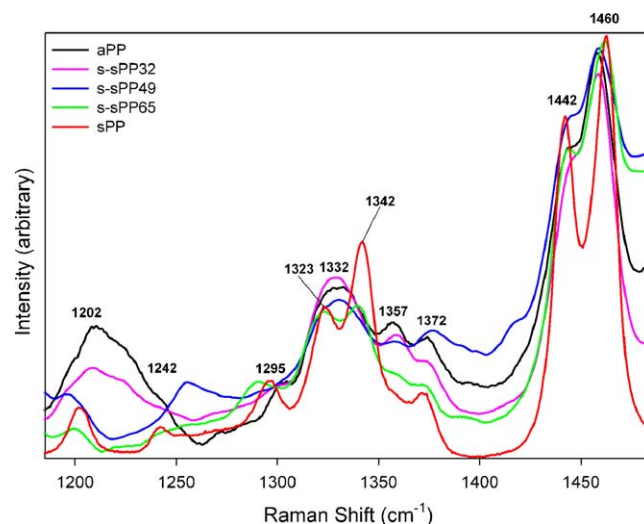


Fig. 6. Raman scattering spectra of melt-slow-cooled semi-syndiotactic polypropylene films in the Raman shift region from 1185 to 1485  $\text{cm}^{-1}$ .

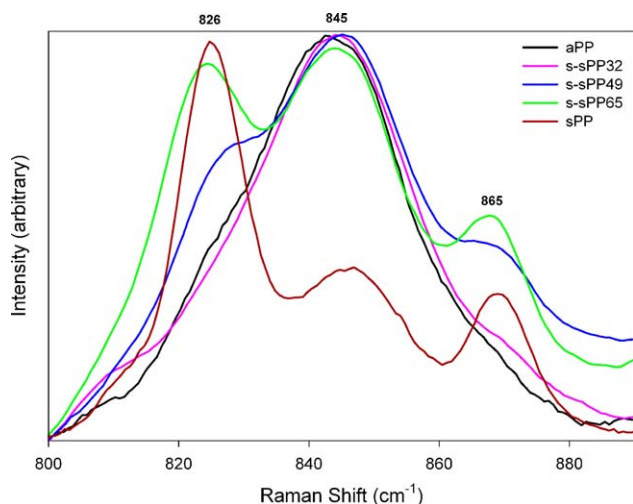


Fig. 4. Raman scattering spectra of melt-slow-cooled semi-syndiotactic polypropylene films in the Raman shift region from 800 to 890  $\text{cm}^{-1}$ .

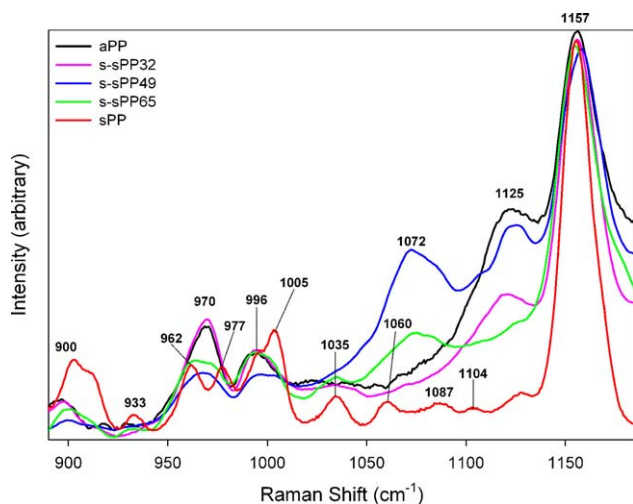


Fig. 5. Raman scattering spectra of melt-slow-cooled semi-syndiotactic polypropylene films in the Raman shift region from 890 to 1185  $\text{cm}^{-1}$ .

theoretical limits of 290 and 310  $\text{cm}^{-1}$  depending of the amount of configurational defects present. sPP chains with fewer errors will generate this band at greater wavenumbers. The spectra in Fig. 2 show excellent correlation with this indexing, from sPP (whose peak appears at 313  $\text{cm}^{-1}$ ) to s-sPP32 (at 303  $\text{cm}^{-1}$ ). Apparently, aPP contains too many defects to compose even the shortest helical sequence theoretically necessary,  $(ggtt)_4$ , to produce the peak. The small peak at 375  $\text{cm}^{-1}$  represents an IR-active  $\angle C-C-C$  bending mode in planar zigzag chains. As mentioned in the previous section, only the most stereoregular materials will be capable of producing a sufficient amount of planar zigzags to emit a strong signal at this band. Weak signals observed in the 400–500  $\text{cm}^{-1}$  range are most likely due to *meso* insertion errors, since peaks characteristic of isotactic polypropylene have been identified near 400 and 460  $\text{cm}^{-1}$  [52,68].

### 3.2.2. 500–800 $\text{cm}^{-1}$ (Fig. 3)

A band near 550  $\text{cm}^{-1}$  is observed in all five spectra. As syndiotacticity increases, the peak gradually transitions from a broad band (in aPP) into a sharp peak with a shoulder at 537  $\text{cm}^{-1}$  (in sPP). Valence force calculations predict skeletal bending modes at 537 and 542  $\text{cm}^{-1}$  for helical sPP [69]. Our results suggest that the peak observed near 550  $\text{cm}^{-1}$  is also sensitive to amorphous chains, by virtue of its presence in every sample. Also, at the highest tacticities (s-sPP65 and sPP), an IR-active helical band appears at 776  $\text{cm}^{-1}$ . In light of X-ray diffractometry results, we suggest that helical bands appearing only in the most stereoregular samples are likely sensitive to helices that compose Form I crystals.

### 3.2.3. 800–900 $\text{cm}^{-1}$ (Fig. 4)

This region contains three methylene rocking bands that quantify the relative content of each chain configuration. Hahn et al. have shown peaks at 826, 845, and 865  $\text{cm}^{-1}$  to be very sensitive to helical, amorphous, and planar zigzag content, respectively [67]. Our results agree very well with these

Table 3  
Vibrational assignments of characteristic syndiotactic vibrational bands<sup>a</sup>

Position (cm <sup>-1</sup> )	Observed activity	Morphology	Comments
303–313	Raman		Syndiotacticity index
375		Planar zigzag	
400–460	Raman		Isotactic content
537	Raman	Helical (cryst.)	Shoulder of 550 cm <sup>-1</sup>
550	Raman	Helical (cryst.) + amorphous <sup>b</sup>	
776	Raman	Helical (cryst.)	
812	IR	Helical (cryst.) <sup>c</sup>	
826	Raman	Helical	
828	IR	Planar (mesophase) <sup>c</sup>	Very weak
843	IR	Helical (mesophase) <sup>c</sup>	Very weak
845	Raman	Amorphous	
865	Raman	Planar zigzag	
867	IR	Helical (cryst.) <sup>c</sup>	
889	IR		IR: split from 900 cm <sup>-1</sup> (?)
900	IR/Raman	Helical (cryst.) <sup>c</sup> + amorphous <sup>b</sup>	IR: parent of 889, 909 cm <sup>-1</sup> (?)
909	IR		IR: split from 900 cm <sup>-1</sup> (?)
933	IR/Raman	Helical (cryst.) <sup>b</sup>	
962	IR/Raman	Planar zigzag (mesophase) <sup>c</sup>	IR: split from 970 cm <sup>-1</sup> Conformation index with 977 cm <sup>-1</sup>
970	IR/Raman	Amorphous	IR: parent of 962, 977 cm <sup>-1</sup>
977	IR/Raman	Helical (mesophase) <sup>c</sup>	IR: split from 970 cm <sup>-1</sup> Conformation index with 962 cm <sup>-1</sup>
992	IR	Helical (amorph.) <sup>b</sup>	
996	IR/Raman	Amorphous	
1005	IR/Raman	Helical (cryst.) <sup>c</sup>	
1035	IR/Raman	Helical (cryst.) <sup>b</sup>	
1060	IR/Raman	Helical (cryst.) <sup>b</sup>	
1072	Raman	Amorphous	
1087	IR/Raman	Helical (cryst.) <sup>b</sup>	
1104	Raman	Helical (cryst.) <sup>b</sup>	
1125	Raman	Amorphous	
1131	IR	Planar zigzag (amorph.) <sup>c</sup>	
1153	IR	Planar zigzag (amorph.) <sup>b</sup>	Split from 1157 cm <sup>-1</sup>
1157	IR/Raman	Non-conformed chains	Normalization/reference peak Parent of 1153, 1169 cm <sup>-1</sup>
1169	IR	Helical (amorph.) <sup>b</sup>	Split from 1157 cm <sup>-1</sup>
1202	IR/Raman	Helical	Syndiotacticity index <sup>b</sup>
1232	IR	Planar zigzag + amorphous	Syndiotacticity index <sup>b</sup> with 1249 cm <sup>-1</sup>
1242	Raman	Helical (cryst.) <sup>b</sup>	
1249	IR	Amorphous	Syndiotacticity index <sup>b</sup> with 1232 cm <sup>-1</sup>
1264	IR	Helical (cryst.) <sup>b</sup>	
1295	Raman	Helical (cryst.) <sup>b</sup>	
1323	IR/Raman	Planar zigzag (mesophase?) <sup>b</sup>	Raman: split from 1332 cm <sup>-1</sup> Analogous to 962 cm <sup>-1</sup>
1332	Raman	Amorphous <sup>b</sup>	Raman: parent of 1323, 1342 cm <sup>-1</sup> Analogous to 970 cm <sup>-1</sup>
1342	Raman	Helical (mesophase?) <sup>b</sup>	Raman: split from 1332 cm <sup>-1</sup> Analogous to 977 cm <sup>-1</sup>
1357	Raman	Amorphous <sup>b</sup>	
1372	Raman	Helical (cryst.) <sup>b</sup>	
1442	Raman	Helical (cryst.) <sup>b</sup>	
1460	IR/Raman	Amorphous	

<sup>a</sup> Assignment taken from valence force calculations [69], unless otherwise noted.

<sup>b</sup> Assignment suggested pursuant to the present work.

<sup>c</sup> Assignment suggested from rheo-FTIR spectroscopy of sPP [54].

findings. A trend is observed in Fig. 4, where less syndiotactic materials (aPP and s-sPP32) are dominated by a broad amorphous response, while the aforementioned peaks are clearly resolved in the more syndiotactic species. s-sPP49 shows a predominant amorphous peak with shoulders on either side. For s-sPP65, helical and amorphous content are nearly

equivalent. Finally, in highly syndiotactic sPP, the helical band is the most intense of the three, with nearly equal amorphous and planar zigzag populations. These results are intuitive, as more stereoregular materials are capable of forming greater populations of conformed chains, as discussed previously in Section 2.

### 3.2.4. 900–1200 $\text{cm}^{-1}$ (Fig. 5)

This region is dominated by responses from IR-active bands, and thus, appears very similar to IR spectra reported in the section to follow. The peak near 900  $\text{cm}^{-1}$  appears to be sensitive both to helical and to amorphous content. Similar to the 550  $\text{cm}^{-1}$  band, it appears even in aPP, but grows sharper and more intense as syndiotacticity increases. The band at 933  $\text{cm}^{-1}$  mimics the behavior of 776  $\text{cm}^{-1}$ , appearing only in the most stereoregular samples. As tacticity increases, the peak at 970  $\text{cm}^{-1}$  appears to “split” into planar zigzag (962  $\text{cm}^{-1}$ ) and helical (977  $\text{cm}^{-1}$ ) components. Concurrently, the peak at 996  $\text{cm}^{-1}$  decreases in intensity, ultimately becoming a shoulder for the helical peak at 1004  $\text{cm}^{-1}$ . IR peaks at similar positions behave almost identically. Additionally, multiple weak C–C skeletal stretching bands appear in sPP only (1035, 1060, 1087, 1104  $\text{cm}^{-1}$ ). The broad peak at 1072  $\text{cm}^{-1}$  is unique in that it is entirely absent at low tacticity, most intense in s-sPP49, and diminishing as tacticity is further increased. This suggests that 1072  $\text{cm}^{-1}$  is very sensitive to helical peaks present in non-crystalline domains, since helices are almost entirely absent in aPP and s-sPP32, yet they participate in Form I crystallite formation to a large extent in s-sPP65 and sPP (as evidenced in X-ray diffractograms). The weak band around 1125  $\text{cm}^{-1}$  appears to be sensitive to amorphous content, diminishing with increased stereoregularity. The strong peak near 1157  $\text{cm}^{-1}$  has been identified as insensitive to polypropylene configuration and conformation [77]. Its appearance simply confirms the presence of polypropylene, and its intensity is often used as a normalization factor for other peaks.

### 3.2.5. 1200–1500 $\text{cm}^{-1}$ (Fig. 6)

Moderately weak peaks at 1202, 1242, 1295, and 1372  $\text{cm}^{-1}$  behave much like 550 and 776  $\text{cm}^{-1}$ —highly sensitive to helical chains, most likely in Form I crystallites due to their absence in less syndiotactic materials (s-sPP49 and lower). An amorphous peak at 1332  $\text{cm}^{-1}$  behaves much like 970  $\text{cm}^{-1}$  and splits into two separate peaks (1323 and 1342  $\text{cm}^{-1}$ ) at greater tacticities. A peak observed at 1357  $\text{cm}^{-1}$  also appears sensitive to amorphous change, as its relative intensity increases with decreasing stereoregularity. Finally, a strong amorphous band is observed at 1460  $\text{cm}^{-1}$ , apparently with a Form-I-sensitive shoulder at 1442  $\text{cm}^{-1}$  that becomes a comparably strong peak in sPP.

## 3.3. FTIR spectroscopy

High-resolution IR absorbance spectra in the wavenumber range from 1300 to 800  $\text{cm}^{-1}$  for all six materials are given in Fig. 7. Each peak is labeled with its center wavenumber position, followed parenthetically by the peak intensity relative to that of the conformation-insensitive peak near 1157  $\text{cm}^{-1}$  [78]. Peak analysis is summarized in Table 3. Several different peak behaviors are observed as tacticity varies:

1. Resolution or “splitting” of one peak into multiple peaks.
2. Horizontal shift in the center wavenumber position.
3. Peak intensity change.

### 3.3.1. Peak splitting

The IR spectra reported include three instances where a single peak appears to split into multiple peaks as syndiotacticity is increased. One such peak is 972  $\text{cm}^{-1}$  (in Fig. 7a and b), which ultimately splits into 978 and 963  $\text{cm}^{-1}$  (in Fig. 7f). Splitting is often a result of different chain types participating in a common domain or local environment. Results from previous IRLD experiments suggest that these two peaks represent planar zigzag (963  $\text{cm}^{-1}$ ) and helical (978  $\text{cm}^{-1}$ ) chains present in a non-crystalline environment that ultimately participate in the interfacial mesophase formed upon sufficient tensile drawing [54]. The absorbance ratio of 978–963  $\text{cm}^{-1}$  is often used to quantify the overall relative population of helical to planar zigzag chains in sPP [77]. The conformation-insensitive reference peak at 1157  $\text{cm}^{-1}$  also splits into three separate, yet somewhat coalesced, peaks (Fig. 7f). The valence force predictions of Schachtschneider and Snyder identify both a helical and planar zigzag peak very near the observed split peaks at 1168.6 and 1153.6  $\text{cm}^{-1}$ , respectively [69]. Again, referring to previous results of sPP dichroism behavior, we suggest that the reference peak characterizes amorphous domains that do not participate in any ordered structure. Using an interpretation similar to that of the 972  $\text{cm}^{-1}$  peak, the reference peak behavior in sPP suggests that a slightly greater population of planar zigzag chains exists overall in disordered domains. This is supported by the X-ray diffractograms reported earlier (Fig. 1) and other IR peaks (812, 867 and 1005  $\text{cm}^{-1}$ ) that show evidence that a significant portion of helical chains reside in ordered environments. Moreover, we suggest that the intermediate split peak at 1161.3  $\text{cm}^{-1}$  represents non-conformed, amorphous chains. This supports descriptions of the mesophase as “partially ordered” and “paracrystalline”, since 972  $\text{cm}^{-1}$  produces no such intermediate amorphous peak upon splitting. It is not clear why the 1157  $\text{cm}^{-1}$  peak splits only for sPP while 972  $\text{cm}^{-1}$  appears to split even in the less stereoregular s-sPP49 sample (Fig. 7c). Though there is no certain crystallographic evidence of an ordered mesophase in these melt-slow-cooled samples, there are perhaps growing populations of helices and planar zigzags inhabiting the slightly more ordered crystalline–amorphous interface, capable of forming the intermediate mesomorph with sufficient external perturbation.

The most curious split appears around 900  $\text{cm}^{-1}$ . Unlike previous instances, this split is most pronounced in s-sPP49 (Fig. 7c) and less so in s-sPP32 (Fig. 7b). There is uncertainty as to whether this is a true split or if shoulders are simply appearing at 889 and 909  $\text{cm}^{-1}$ . The latter case may be reinforced by the fact that the IRLD behavior of 900  $\text{cm}^{-1}$  suggests that it is sensitive to Form I crystallites, which are composed of only helices. Regardless, it is of peculiar interest, since IR peaks at both positions have been, to our knowledge, neither predicted nor observed. It is also tempting to speculate that the anomalous behavior in the X-ray diffractogram and IR spectrum of s-sPP49 are somehow related. The intermediate level of stereoregularity present in s-sPP49 hints at a threshold below which helices and planar zigzags cannot form. Perhaps

s-sPP49 possesses some “critical” level of stereoregularity necessary to form a non-ideal, disordered, or metastable crystal morph that would cause the  $900\text{ cm}^{-1}$  peak splitting and unidentified X-ray diffraction peaks. To confirm this, however, a more thorough crystallographic analysis is needed. Finally, the  $996.9\text{ cm}^{-1}$  peak in s-sPP32 (Fig. 7b) appears to split into  $992.5$  and  $1004.9\text{ cm}^{-1}$  at greater tacticity. The literature does define two distinct vibrational bands near these peak positions; thus, it is uncertain whether or not this is a true split [69]. Moreover, a complementary work studying thermal effects on IR spectra of semi-sPP reports that the two split peaks do not appear to coalesce into a parent peak as temperature increases [79]. Therefore, it is suggested that  $992.5$  and  $1004.9\text{ cm}^{-1}$  are, indeed, distinct peaks. Also, as syndiotacticity increases, the lower-energy band decreases in intensity until it no longer appears in sPP (Fig. 7f). Based on this result, we assign the

bands near  $992$  and  $1005\text{ cm}^{-1}$  to helical chains present in amorphous and Form I crystalline domains, respectively.

### 3.3.2. Peak wavenumber shifting

Certain IR bands undergo slight changes in their center wavenumber position as syndiotacticity varies. Two different trends are observed based on peak type. Peaks resulting from a split continue to migrate away from the parent peak as syndiotacticity increases. For example, the peaks resulting from the  $972\text{ cm}^{-1}$  split migrate from  $977.0\text{ cm}^{-1}$  and  $963.6\text{ cm}^{-1}$  (Fig. 7d) to  $978.0\text{ cm}^{-1}$  and  $963.1\text{ cm}^{-1}$ , respectively (Fig. 7f). Other peaks show a gradual move to greater wavenumbers with increasing syndiotacticity, such as:

1.  $840.9\text{ cm}^{-1}$  (Fig. 7a)  $\rightarrow$   $842.8\text{ cm}^{-1}$  (Fig. 7f).
2.  $898.4\text{ cm}^{-1}$  (Fig. 7a)  $\rightarrow$   $905.4\text{ cm}^{-1}$  (Fig. 7f).

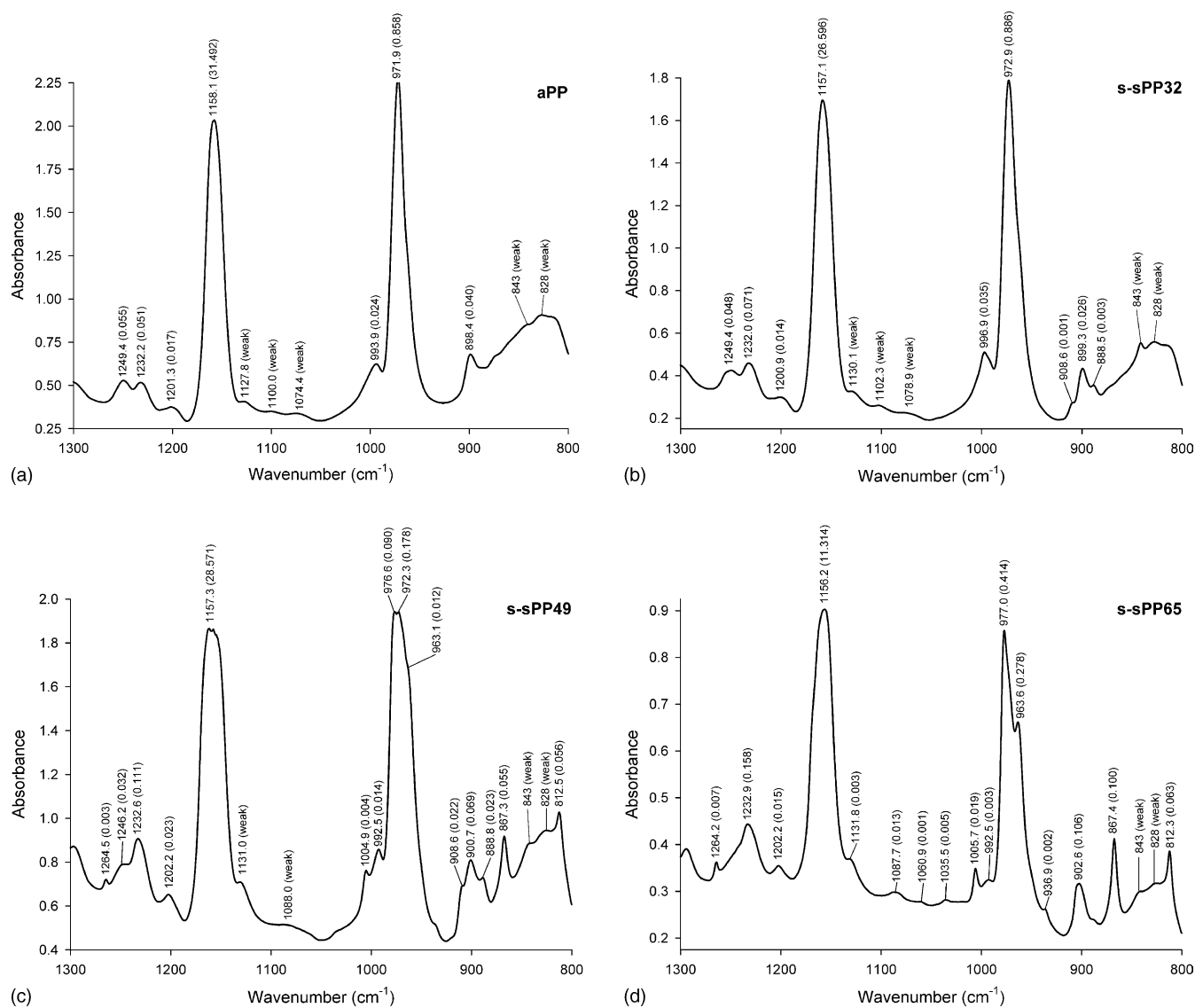


Fig. 7. FTIR absorbance spectra of melt-slow-cooled semi-syndiotactic polypropylene films in the range from  $1300$  to  $800\text{ cm}^{-1}$ . Spectra are collected at a resolution of  $0.5\text{ cm}^{-1}$  with 1024 transients co-added. Each peak is labeled with two values: center wavenumber position and, parenthetically, peak area intensity normalized by that of the  $1157\text{ cm}^{-1}$  reference peak [78]. Key: (a) aPP; (b) s-sPP32; (c) s-sPP49; (d) s-sPP65; (e) s-sPP67; (f) sPP.

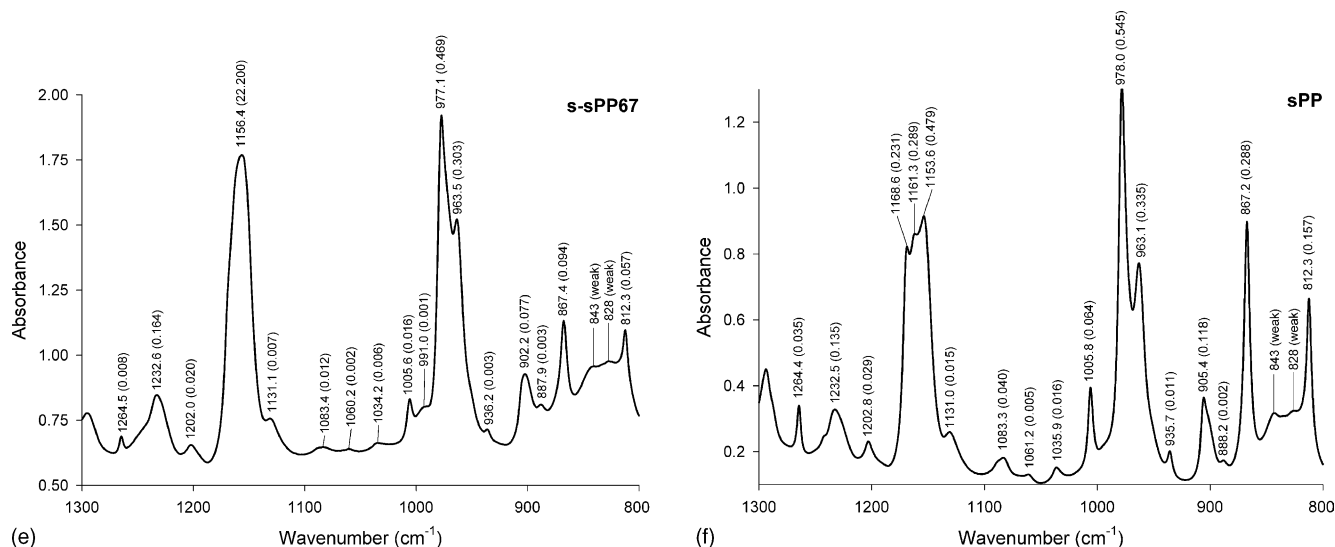


Fig. 7. (Continued).

3. 971.9 cm<sup>-1</sup> (Fig. 7a) → 972.9 cm<sup>-1</sup> (Fig. 7b, prior to splitting).
4. 1201.3 cm<sup>-1</sup> (Fig. 7a) → 1202.8 cm<sup>-1</sup> (Fig. 7f).

The reference peak at 1157 cm<sup>-1</sup> (Fig. 7a), however, shows opposite behavior, shifting as far as 1156.2 cm<sup>-1</sup> (Fig. 7d) prior to splitting. This is most likely due to the greater population of amorphous helices that eventually appear in sPP after splitting (1153.6 cm<sup>-1</sup> in Fig. 7f). In general, peak shifting is due to a change in local environment (intramolecular and intermolecular interactions) resulting from variance in molecular order [77]. As stereoregularity increases, samples possess chains that are in ever more organized arrangements. This results in the need for slightly more energetic quanta to facilitate vibrational excitation.

### 3.3.3. Relative peak intensity change

The most basic variation in spectra is that of peak intensity (size, shape, width). In general, peak intensity is proportional to the population of a specific component within the species analyzed. The following intensity change trends are observed in Fig. 7 as syndiotacticity increases:

1. Increase in non-crystalline helices (812 and 977 cm<sup>-1</sup>).
2. Increase in Form I crystallites (867, 900, 1005, 1264, small peaks in the range from 1030 to 1100 cm<sup>-1</sup>).
3. Decrease in amorphous chains (992 and 1249 cm<sup>-1</sup>).
4. Increase in planar zigzags (963, 1131 and 1232 cm<sup>-1</sup>).

These trends are expected, since materials with greater molecular order are more able to produce ordered structures at greater length scales. Also, it appears that the absorbance ratio of 1232–1249 cm<sup>-1</sup> may also be used as a syndiotacticity index. In aPP (Fig. 7a), the peaks are of nearly equal magnitude. As syndiotacticity increases, 1249 cm<sup>-1</sup> decreases steadily until it becomes a shoulder of 1232 cm<sup>-1</sup>. Two very weak peaks near 828 and 843 cm<sup>-1</sup> also appear to shift slightly and change intensity as syndiotacticity varies. While weak in absorbance

spectra, these peaks have demonstrated very strong dichroic behavior, which has aided in characterizing them as planar zigzag and helical bands, respectively, that are sensitive to the mesophase.

## 4. Conclusion

The role of tacticity on vibrational spectra has been studied for a series of well-defined, metallocene-catalyzed, semi-syndiotactic polypropylenes with stereoregular content ranging from 26 to 96% *rr*. High-resolution IR absorbance spectra prove to be sensitive to tacticity changes in melt-slow-cooled films. This is reflected in the trends of peak splitting, wavenumber shifting, and relative intensity change in spectra as syndiotacticity increases. Supported by results from X-ray diffractometry and Raman spectroscopy, IR absorbance spectra show that materials of greater stereoregularity are, intuitively, more capable of arranging molecular chains into ordered structures—helical, planar zigzag, and non-conformed chains into different domains (amorphous, interfacial/mesophase).

s-sPP49, a sample of moderate stereoregularity, gives peculiar results in its X-ray powder diffractogram and IR absorbance spectrum. In both measurements, new peaks appear that have not been identified with known sPP morphology. It is interesting to note that, as syndiotacticity increases, spectral peaks indicative of (*ggtt*)<sub>n</sub> helices first appear (although weakly) in s-sPP49. For crystallographic measurements, a more detailed study needs to be undertaken. In the IR spectrum of s-sPP49, peak behavior near 900 cm<sup>-1</sup> appears ostensibly similar to splitting that occurs at 972 cm<sup>-1</sup>. Previous IR dichroism analysis of sPP identifies 900 cm<sup>-1</sup> as sensitive to helical Form I crystals. Thus, it is suggested that helical chains in different, as-yet unidentified, disordered Form I modifications—and not chains of different conformations, as in the crystalline–amorphous interfacial domain—are causing this strange behavior.

With a more thorough understanding of the influence of tacticity of vibrational spectra, we hope to be able to resolve

and interpret better the IR linear dichroism spectra of these and other stereoregular materials as collected using rheo-FTIR spectroscopy [57]. Results from this work will be critical in distinguishing stereoregularity effects from peak shifting, splitting, and intensity changes due to tensile perturbation, all of which have been observed previously [54,80]. Also, an analogous work investigating the effects of temperature on the IR spectra of semi-sPP has been completed recently [79].

## Acknowledgments

The authors recognize extensive assistance and helpful discussions from Dr. D. Haddad (Wayne State U.) regarding Raman spectroscopy measurements. We also express gratitude to Dr. S. Venkataramani (3M Co.) for performing GPC measurement and analysis of sPP. This work is supported financially by NSF-CAREER (DMR9876221) and NSF-IGERT (DGE9870720).

## References

- [1] C. Duchesne, X. Kong, J. Brisson, M. Pézolet, R.E. Prud'homme, *Macromolecules* 35 (2002) 8768.
- [2] S. Nomura, R. Ashitani, H. Matsuda, L. Banda, *Polymer* 42 (2001) 9045.
- [3] D.K. Graff, H. Wang, R.A. Palmer, J.R. Schoonover, *Macromolecules* 32 (1999) 7147.
- [4] H.V. Shah, C.J. Manning, G.A. Arbuckle, *Appl. Spectrosc.* 53 (1999) 1542.
- [5] T. Buffeteau, M. Pézolet, *Macromolecules* 31 (1998) 2631.
- [6] M. Sonoyama, K. Shoda, G. Katagiri, H. Ishida, T. Nakano, S. Shimada, T. Yokoyama, H. Toriumi, *Appl. Spectrosc.* 51 (1997) 598.
- [7] C. Hayes, E. Mendes, L. Bokobza, F. Boué, L. Monnerie, *Macromol. Symp.* 94 (1995) 227.
- [8] V.G. Gregoriou, I. Noda, A.E. Dowrey, C. Marcott, J.L. Chao, R.A. Palmer, *J. Polym. Sci. Part B: Polym. Phys.* 31 (1993) 1769.
- [9] R.D.B. Fraser, *J. Chem. Phys.* 21 (1953) 381.
- [10] R.D.B. Fraser, *J. Chem. Phys.* 24 (1956) 89.
- [11] R.S. Stein, *J. Polym. Sci.* 31 (1958) 327.
- [12] R.S. Stein, F.H. Norris, *J. Polym. Sci.* 21 (1956) 381.
- [13] G. Voyiatzis, G. Petekidis, D. Vlassopoulos, E.I. Kamitsos, A. Brugge-man, *Macromolecules* 29 (1996) 2244.
- [14] K. Huang, L.A. Archer, G.G. Fuller, *Macromolecules* 29 (1996) 966.
- [15] G. Natta, P. Corradini, P. Ganis, *Makromol. Chem.* 39 (1960) 238.
- [16] G. Natta, P. Corradini, P. Ganis, *J. Polym. Sci.* 58 (1962) 1191.
- [17] G. Natta, M. Peraldo, G. Allegra, *Makromol. Chem.* 75 (1964) 215.
- [18] J.A. Ewen, R.L. Jones, A. Razavi, J.D. Ferrara, *J. Am. Chem. Soc.* 110 (1988) 6255.
- [19] P. Longo, A. Proto, A. Grassi, P. Ammendola, *Macromolecules* 24 (1991) 4624.
- [20] Y. Chatani, H. Maruyama, T. Asanuma, T. Shiomura, *J. Polym. Sci. Part B: Polym. Phys.* 29 (1991) 1649.
- [21] C. De Rosa, F. Auriemma, V. Vinti, *Macromolecules* 30 (1997) 4137.
- [22] B. Lotz, A.J. Lovinger, R.E. Cais, *Macromolecules* 21 (1988) 2375.
- [23] Y. Chatani, H. Maruyama, K. Noguchi, T. Asanuma, T. Shiomura, *J. Polym. Sci. Part C: Polym. Lett.* 28 (1990) 393.
- [24] A.J. Lovinger, B. Lotz, D.D. Davis, *Polymer* 31 (1990) 2253.
- [25] C. De Rosa, P. Corradini, *Macromolecules* 26 (1993) 5711.
- [26] A.J. Lovinger, B. Lotz, D.D. Davis, M. Schumacher, *Macromolecules* 27 (1994) 6603.
- [27] K. Crämer, M. Schneider, R. Mülhaupt, H.-J. Cantow, S.N. Magonov, *Polym. Bull.* 32 (1994) 637.
- [28] R. Thomann, C. Wang, J. Kressler, S. Jüngling, R. Mülhaupt, *Polymer* 36 (1995) 3795.
- [29] J. Rodriguez-Arnold, Z. Bu, S.Z.D. Cheng, *J. Macromol. Sci. -Rev. Macromol. Chem. Phys.* C35 (1995) 117.
- [30] C. De Rosa, F. Auriemma, P. Corradini, *Macromolecules* 29 (1996) 7452.
- [31] D.J. Lacks, *Macromolecules* 29 (1996) 1849.
- [32] Z. Bu, Y. Yoon, R.-M. Ho, W. Zhou, I. Jangchud, R.K. Eby, S.Z.D. Cheng, E.T. Hsieh, T.W. Johnson, R.G. Geerts, S.J. Palackal, G.R. Hawley, M.B. Welch, *Macromolecules* 29 (1996) 6575.
- [33] K. Palmo, S. Krimm, *Macromolecules* 29 (1996) 8549.
- [34] B. Pirozzi, R. Napolitano, *Eur. Polym. J.* 28 (1992) 703.
- [35] A. Bunn, M.E.A. Cudby, R.K. Harris, K.J. Packer, B.J. Say, *J. Chem. Soc., Chem. Commun.* (1981) 15.
- [36] P. Sozzani, R. Simonutti, M. Galimberti, *Macromolecules* 26 (1993) 5782.
- [37] W. Stocker, M. Schumacher, S. Graff, J. Lang, J.C. Wittmann, A.J. Lovinger, B. Lotz, *Macromolecules* 27 (1994) 6948.
- [38] P. Sozzani, R. Simonutti, A. Comotti, *Magn. Reson. Chem.* 32 (1994) S45.
- [39] F. Auriemma, C. De Rosa, O. Ruiz de Ballesteros, P. Corradini, *Macromolecules* 30 (1997) 6586.
- [40] B. Lotz, C. Mathieu, A. Thierry, A.J. Lovinger, C. De Rosa, O. Ruiz de Ballesteros, F. Auriemma, *Macromolecules* 31 (1998) 9253.
- [41] R. Napolitano, B. Pirozzi, *Macromolecules* 31 (1998) 3626.
- [42] R.-D. Maier, R. Thomann, J. Kressler, R. Mülhaupt, B. Rudolf, *J. Polym. Sci. Part B: Polym. Phys.* 35 (1997) 1135.
- [43] R. Silvestri, P. Sgarzi, *Polymer* 39 (1998) 5871.
- [44] T.C. Clancy, M. Pütz, J.D. Weinhold, J.G. Curro, W.L. Mattice, *Macromolecules* 33 (2000) 9452.
- [45] F. Auriemma, O. Ruiz de Ballesteros, C. De Rosa, *Macromolecules* 34 (2001) 4485.
- [46] C. De Rosa, M.C. Gargiulo, F. Auriemma, O. Ruiz de Ballesteros, A. Razavi, *Macromolecules* 35 (2002) 9083.
- [47] L. Guadagno, C. D'Aniello, C. Naddeo, V. Vittoria, S.V. Meille, *Macromolecules* 35 (2002) 3921.
- [48] T. Nakaoki, T. Yamanaka, Y. Ohira, F. Horii, *Macromolecules* 33 (2000) 2718.
- [49] L. Guadagno, L. D'Arienzo, V. Vittoria, *Macromol. Chem. Phys.* 201 (2000) 246.
- [50] T. Ishioka, N. Masaoka, *Polymer* 43 (2002) 4639.
- [51] V.G. Gregoriou, G. Kandilioti, K.G. Gatos, *Vib. Spectrosc.* 34 (2004) 47.
- [52] G. Masetti, F. Cabassi, G. Zerbi, *Polymer* 21 (1980) 143.
- [53] J. Jin, H. Lim, S.S. Kim, K. Song, *Polymer (Korea)* 26 (2002) 745.
- [54] M.S. Sevegney, G. Parthasarthy, R.M. Kannan, D.W. Thurman, L. Fernandez-Ballester, *Macromolecules* 36 (2003) 6472.
- [55] K. Song, J. Ok, *Abstr. Pap. Am. Chem. Soc.* 213 (1997) 38.
- [56] V. Vittoria, L. Guadagno, A. Comotti, R. Simonutti, F. Auriemma, C. De Rosa, *Macromolecules* 33 (2000) 6200.
- [57] G.R. Hofmann, M.S. Sevegney, R.M. Kannan, *Int. J. Polym. Anal. Charact.* 9 (2004) 245.
- [58] L. Guadagno, C. D'Aniello, C. Naddeo, V. Vittoria, *Macromolecules* 33 (2000) 6023.
- [59] L. Guadagno, C. D'Aniello, C. Naddeo, V. Vittoria, *Macromolecules* 34 (2001) 2512.
- [60] M.S. Sevegney, Ph.D. Dissertation, Wayne State University, 2004.
- [61] A.R. Siedle, in press.
- [62] A.R. Siedle, R.A. Newmark, B.F. Duerr, P.C. Leung, *J. Mol. Catal. A: Chem.* 214 (2004) 187.
- [63] E.D. Carlson, M.T. Krejchi, C.D. Shah, T. Terakawa, R.M. Waymouth, G.G. Fuller, *Macromolecules* 31 (1998) 5343.
- [64] A.R. Khare, S.Y. Ding, M.T.K. Ling, C. Qin, L. Woo, *Thermochim. Acta* 367 (2001) 119.
- [65] R. Inapagolla, R.M. Kannan, W. Wiyatno, G.G. Fuller, R.M. Waymouth, in preparation.
- [66] C. De Rosa, F. Auriemma, O. Ruiz de Ballesteros, *Macromolecules* 36 (2003) 7607.
- [67] T. Hahn, W. Suen, S. Kang, S.L. Hsu, H.D. Stidham, A.R. Siedle, *Polymer* 42 (2001) 5813.
- [68] S.L. Hsu, T. Hahn, W. Suen, S. Kang, H.D. Stidham, A.R. Siedle, *Macromolecules* 34 (2001) 3376.
- [69] J.H. Schachtschneider, R.G. Snyder, *Spectrochim. Acta* 21 (1965) 1527.

- [70] Polymer synthesis is described by: A.R. Siedle, D.K. Misemer, V.V. Kolpe, B.F. Duerr, U.S. Patents 6,265,512, 6,323,151, 6,429,274, 6,448,358.
- [71] While this post-press annealing/relaxation step is not as crucial here as it is in IRLD experiments, residual processing stress may yet affect vibrational band positions, see: S. Frisk, R.M. Ikeda, J.F. Rabolt, D.B. Chase, *Abstr. Pap. Am. Chem. Soc.* 220 (2000) 200-PMSE.
- [72] F. Auriemma, C. De Rosa, P. Corradini, *Macromolecules* 26 (1993) 5719.
- [73] F. Auriemma, R. Born, H.W. Spiess, C. De Rosa, P. Corradini, *Macromolecules* 28 (1995) 6902.
- [74] C. De Rosa, F. Auriemma, O. Ruiz de Ballesteros, *Polymer* 42 (2001) 9729.
- [75] A.J. Lovinger, B. Lotz, D.D. Davis, F.J. Padden Jr., *Macromolecules* 26 (1993) 3494.
- [76] The Raman spectra of s-sPP67 is nearly identical to that of s-sPP65, and is thus not reported here.
- [77] J.L. Koenig, L.E. Wolfram, J.G. Grasselli, *Spectrochim. Acta* 22 (1966) 1233.
- [78] The parenthetical value given for the  $1157\text{ cm}^{-1}$  peak in each Fig. 7 spectrum is the absolute peak area.
- [79] M.S. Sevegney, R.M. Kannan, A.R. Siedle, P.A. Percha, *J. Polym. Sci. Part B: Polym. Phys.* 43 (2005) 439.
- [80] G. Parthasarthy, M.S. Sevegney, R.M. Kannan, *J. Polym. Sci. Part B: Polym. Phys.* 40 (2002) 2539.